



**HAL**  
open science

## Tensegrity laboratory drilling rig for earth and space drilling, mining, and exploration

Mohamed S Khaled, Muhao Chen, Enrique Z Losoya, Luis A Rodriguez, Eduardo Gildin, Robert E Skelton

► **To cite this version:**

Mohamed S Khaled, Muhao Chen, Enrique Z Losoya, Luis A Rodriguez, Eduardo Gildin, et al.. Tensegrity laboratory drilling rig for earth and space drilling, mining, and exploration. International Journal of Solids and Structures, In press. hal-03266625

**HAL Id: hal-03266625**

**<https://hal.science/hal-03266625>**

Submitted on 22 Jun 2021

**HAL** is a multi-disciplinary open access archive for the deposit and dissemination of scientific research documents, whether they are published or not. The documents may come from teaching and research institutions in France or abroad, or from public or private research centers.

L'archive ouverte pluridisciplinaire **HAL**, est destinée au dépôt et à la diffusion de documents scientifiques de niveau recherche, publiés ou non, émanant des établissements d'enseignement et de recherche français ou étrangers, des laboratoires publics ou privés.

# Tensegrity laboratory drilling rig for earth and space drilling, mining, and exploration

Mohamed S. Khaled<sup>a,1</sup>, Muhao Chen<sup>b,2</sup>, Enrique Z. Losoya<sup>a,1</sup>, Luis A. Rodriguez<sup>c,3</sup>, Eduardo Gildin<sup>a,\*4</sup> and Robert E. Skelton<sup>b,5</sup>

<sup>a</sup>Department of Petroleum Engineering, Texas A&M University, College Station, TX, 77840, USA

<sup>b</sup>Department of Aerospace Engineering, Texas A&M University, College Station, TX, 77840, USA

<sup>c</sup>Department of Mechanical Engineering, Texas A&M University, College Station, TX, 77840, USA

## ARTICLE INFO

### Keywords:

Tensegrity Structure  
Light Weight Drilling Rig  
Space Mining  
Space Drilling

## Abstract


Drilling operations are increasingly becoming a manufacturing process where repeatability, versatility, and speed matter the most for an operator or future space missions. Nonetheless, the ongoing energy transition efforts will undoubtedly shape the objectives and priorities of drilling operators into new markets with unexplored technical challenges, where versatility, mobility, and automated systems will play crucial roles in determining successful applications. This study explores and introduces the application of tensegrity-based structures, commonly used in space exploration, to Earth and Space drilling systems by modeling, designing, and building a tensegrity-based miniature drilling rig. Robust models for designing a drilling rig based on tensegrity structures and anticipated load conditions are presented. In addition, the drilling tests and experimental results described proving that the tensegrity could be applied to unusual applications such as drilling. Furthermore, our models show that constructing a lightweight tensegrity-based structure for drilling applications on Earth and Mars is not only possible but feasible by tuning design variables, such as the structure complexity, bar and string sizes, pre-stress, etc. Ultimately, tensegrity structures allow more volume-efficient, lightweight, and deployable mechanisms, to name a few benefits essential for space deployment and help earth-based systems enhance rig mobility that could reduce drilling cost and the environmental footprint of drilling the Exploration and Production (E&P) industry by downsizing the site's carbon expenditure.

## 1. Introduction

The development of zero carbon emissions cycles in petroleum exploration is paramount to achieve an effective energy transition from the current fossil fuel-based economy. Reducing the footprint of a drilling rig through process digitization (e.g., digital twins and drilling automation) and reducing its environmental impact (e.g., downsizing the site's carbon expenditure) can accelerate reaching this goal. Therefore, the Exploration and Production (E&P) Industry, especially the drilling business, has lately turned to other industries to learn the benefits of early adoption of technologies that can impact the efficiency of oil production and mitigate the environmental impact

of its operations. Particularly, they have turned to the aerospace and manufacturing industries, of which the E&P industry shares several similarities in terms of complexity, high capital expenditure, and uncertainty. We highlight the improved modeling and simulation capabilities derived from case studies [1, 2], the adoption of risk management frameworks from NASA to reduce exposure to uncertainty [3], and the increased use of additive manufacturing to produce components [4]. Other technologies applied to drilling are mechanistic workflows for drilling optimization based on experimental techniques and the use of control and orientation algorithms to determine the bit's position and trajectory [5, 6, 7, 8, 9], which can easily be found in many aerospace applications. On the other hand, developed E&P devices, methods, and modeling techniques coined for extreme environmental conditions with high uncertainty have benefited other industries; improved seismic nodes, airborne magnetic surveys, and advancements on high-temperature high-pressure (HTHP) measurement while drilling tools are some examples of exported technologies from the oil industry [10]. Common extreme conditions faced when drilling on Earth, such as temperatures of up to 180°C, pressures of 15,000 psi, and high-sustained vibrations, resemble those faced in space drilling and exploration [11]. Nonetheless, efficiency, weight, and automation reliability constraints are much more crucial when drilling in space [12, 13, 14]. Both industries could complement and adapt lessons learned from each other while working towards their particular objectives. This study demonstrates the feasibility of designing and

\*Corresponding author

 moh.shafik@tamu.edu (M.S. Khaled); muhaochen@tamu.edu (M.

Chen); ez1@tamu.edu (E.Z. Losoya); lar3763@tamu.edu (L.A. Rodriguez);

egildin@tamu.edu (E. Gildin); bobskelton@tamu.edu (R.E. Skelton)

ORCID(s): 0000-0001-8855-3504 (M.S. Khaled); 0000-0003-1812-6835 (M. Chen); 0000-0001-7763-3349 (E.Z. Losoya); 0000-0003-4679-2739 (L.A. Rodriguez); 0000-0001-5985-4500 (E. Gildin); 0000-0001-6503-9115 (R.E. Skelton)

<sup>1</sup>Graduate Student, Department of Petroleum Engineering, Texas A&M University, College Station, TX, USA.

<sup>2</sup>Postdoctoral Researcher, Department of Aerospace Engineering, Texas A&M University, College Station, TX, USA.

<sup>3</sup>Graduate Student, Department of Mechanical Engineering, Texas A&M University, College Station, TX, USA.

<sup>4</sup>Associate Professor, Department of Petroleum Engineering, Texas A&M University, College Station, TX, USA.

<sup>5</sup>TEES Eminent Professor, Department of Aerospace Engineering, Texas A&M University, College Station, TX, USA.

building a drilling rig using tensegrity structure principles that can aid in drilling under new extreme environments in space and on the Earth.

## Nomenclature

$n_a$	Number of free nodes.
$n_n$	Number of total nodes
$n_e$	Number of structure elements.
$\mathbf{K}$	Structure stiffness matrix.
$\mathbf{C}$	Connectivity matrix of the tensegrity structure.
$\mathbf{E}$	Structure element Young's Modulus vector $\mathbf{E} = [E_1 \ E_2 \ \dots \ E_{n_e}]^T \in \mathbb{R}^{n_e}$ .
$\mathbf{A}$	Structure element cross-section vector $\mathbf{A} = [A_1 \ A_2 \ \dots \ A_{n_e}]^T \in \mathbb{R}^{n_e}$ .
$\mathbf{l}$	Structure element length vector $\mathbf{l} = [l_1 \ l_2 \ \dots \ l_{n_e}]^T \in \mathbb{R}^{n_e}$ .
$\mathbf{n}$	Nodal coordinate vector.
$\mathbf{f}_{ex}$	External forces on the structure nodes.
$\mathbf{m}$	Structure mass vector of each structure member, $\mathbf{m} = [m_1 \ m_2 \ \dots \ m_{n_e}]^T \in \mathbb{R}^{n_e}$ .
$\hat{\bullet}$	An operator that converts a vector into a diagonal matrix.
$[\bullet]$	An operator that only takes the diagonal entries of a matrix.
$b.d.(.)$	An operator that converts each column of the given matrix into a block diagonal matrix.
$\otimes$	The Kronecker product operator.
$\mathbf{x}$	Force density (force per unit length) vector of structure members.
$\mathbf{g}$	The gravity vector ( $g$ is gravity constant).
$\mathbf{a}$	The value of $a_i$ in vector $\mathbf{a} = [a_1 \ a_2 \ \dots \ a_{n_a}]^T \in \mathbb{R}^{n_a}$ are the indices of the free nodes in the nodal coordinate vector $\mathbf{n}$ .
$\mathbf{E}_a$	An orthonormal matrix to abstract free nodes $\mathbf{n}_a$ from nodal vector $\mathbf{n}$ , which satisfies $\mathbf{E}_a(:, i) = \mathbf{I}_{3n}(:, a_i) \in \mathbb{R}^{3n \times n_a}$ and $\mathbf{n}_a = \mathbf{E}_a^T \mathbf{n}$ .

Improvements in drilling performance and cost reductions require integrating and adopting new manufacturing technologies and structural designs to develop reliable, flexible, mobile, and versatile structures to meet our world's demand for energy in an increasingly environmentally conscious way. This paper aims to bring attention to this overlooked component by introducing an emerging structural design technology into the modern drilling rig. In particular, we propose the design of tensegrity-based structures, commonly used in space exploration, to Earth and Space drilling systems by modeling, designing, and building a tensegrity-based miniature drilling rig. The developed drilling rig adopts tensegrity notions to 1) build a lightweight and deployable structure for easier installation in the land (Earth) and in space (Moon/Mars); and for reducing drill site footprint "environmental" and enhancing rig mobility in Earth

under different loading conditions; 2) integrate the tensegrity structure with a rotary drilling mechanism where the bit cuts rock layers by applying rotation and weight from the surface. This drilling methodology could aid in drilling hundreds of meters in the Earth, Moon, and Martian subsurface.

Our novel work presented here demonstrates that the tensegrity-based structure could be applied to unusual applications such as drilling. We obtain robust models that can withstand anticipated load conditions in a variety of environments, ranging from common Earth operations to more complex space explorations. In addition, we describe the entire process of design-built-integrate and test by means of drilling tests and experimental results. Furthermore, our models show that constructing a lightweight tensegrity-based structure for drilling applications on Earth and Mars is not only possible but feasible by tuning design variables, such as the structure complexity, bar and string sizes, pre-stress, among others. Ultimately, tensegrity structures allow more volume-efficient, lightweight, and deployable mechanisms essential for space deployment and Earth applications. To this end, it will also enhance earth-based rig mobility, leading to reduction of drilling costs and environmental footprint of massive drilling rigs mitigation drilling site's carbon expenditure.

This paper is structured as follows: Section 2 presents the governing equations of tensegrity statics and critical buckling analysis. Section 3 shows the mathematical and experimental designs of the Texas A&M University tensegrity drilling rig. Section 4 demonstrates the drilling operation and tests. Section 5 discusses the conclusions and future work.

## 1.1. Related literature

Drilling rigs are typically rotary-typed rigs that use a bit to crush and drill through rock strata to reach a target depth. A modern rotary drilling rig comprises several electrical and mechanical systems, including complex cables, mechanisms, electronics, draw-works, and pumps to control the drilling process below the surface accurately. Several advances have changed some of the key structural and operational components of a drilling rig. For instance, electric power generation and electromechanical systems became operational 40 to 50 years ago, while the use of mobile "land platforms" with one rig drilling several wells on a single pad began around 2013. Another significant development was the inclusion of the top-drive and advanced motion compensation systems for offshore drilling rigs [15]. Over the past decade, advances in drilling structures technology have mainly been focused on improved remote control systems and incremental materials, and manufacturing improvements [16, 17, 18, 19, 20]. Perhaps the most overlooked part of a modern drilling rig is the derrick structural design, as pragmatism and reliability have been the drivers of adoption in the industry, which has led to limited research in this area. Most of today's drilling rigs still follow the same hoist and draw-works rigid structure from the wooden rig used in that famous oil well in Pennsylvania. The traditional derrick shape (as shown in Fig.1) is a lattice structure that

provides the structural support needed to hold the top-drive, drillstring, and other mechanisms in place. Modern rigs are designed for very specific setups and types of operations; most have limited mobile capabilities and are cumbersome to move from one location to another. Furthermore, even fewer commercial investments have been made to study alternative structural solutions that could change the way to drill for energy resources.

Few attempts have been made to build lightweight drilling rig systems; for instance, Wong and Whiteman presented a lightweight drill rod in making drilling string for the use of oil well [21]. Jortveit designed a modular lightweight drilling rig to be placed on a platform deck to support the deck and derrick [22]. Jiang et al. analyzed a lightweight composite carbon fiber drill pipe and compared it with an alloy steel one [23]. Fan et al. designed a lightweight underground drilling rig by using light alloy material for the feeding device [24]. Wang presented a lightweight electric earth drill that is driven by the motor and has low noise, which causes less damage to the health of the workers and does not disturb the residents around the construction site [25]. However, none of the authors start from looking for a lightweight deployable structure paradigm, looking for ways to integrate material architecture choices and control architecture. Biological systems perhaps provide the greatest evidence that the tensegrity paradigm yields the most mass efficient structures that can be used to design our drilling rig structures.

Tensegrity is a coined word: tension and integrity, by [26] for the art form created [27]. The tensegrity system is a stable network of compressive members (bars/struts) and tensile members (strings/cables) [28, 29]. In fact, many macro and microbiological structures are consistent with tensegrity models, such as fishtails [30], animal spines [31], living cells [32], DNA nano bundles [33], etc. After decades study, tensegrity structure has demonstrated its many advantages: 1) Minimum mass structure solutions for five fundamental loading conditions (compression [34], tension [35], cantilever [36], torsion [37], and simply supported [38]), and topology design or form finding approaches for various of structures [39, 40, 41, 42]; 2) Redundant control inputs (both strings and bars can be actuators) provide robustness; 3) The one-dimensional elements results in more accurate model and better performance; 4) Change shape w/o changing stiffness or change stiffness w/o changing shape [43]. Due to these benefits, many robots have been developed using the tensegrity paradigm, such as morphing airfoil/wing [44, 45], robotic fish [46], planetary landers [47, 48]. Due to these many advantages of tensegrity, this paper implements the tensegrity concept to design a deployable drilling rig for space mining.

## 2. Tensegrity rig equilibrium

### 2.1. Nodal coordinates and connectivity matrix

The nodal coordinate vectors describe the tensegrity structure with a total number of nodes  $n_n$ . The coordinates of the  $i$ th ( $i = 1, 2, \dots, n_n$ ) node.  $\mathbf{n}_i \in \mathbb{R}^3$  in the tensegrity

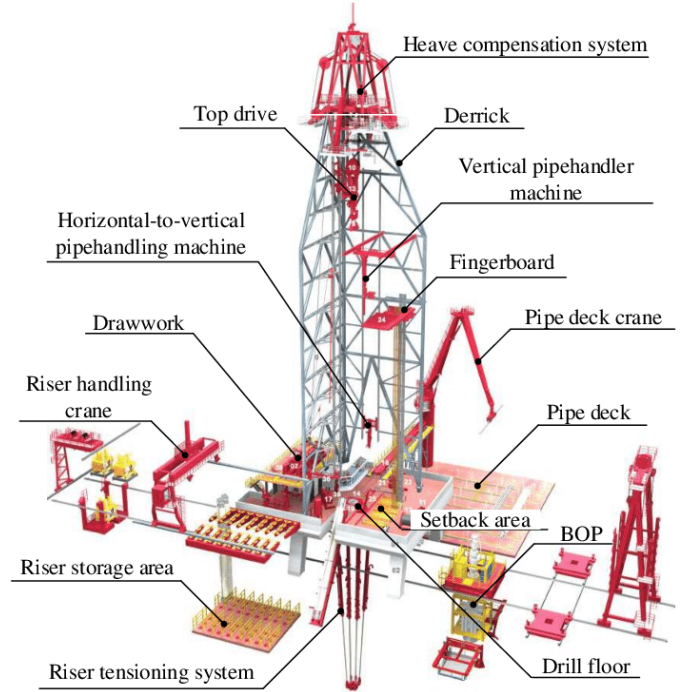


**Figure 1:** Traditional Drilling Rig and Hoist Structure, adapted from [16].

structure are defined as:  $\mathbf{n}_i = [x_i \ y_i \ z_i]^T$ . Then, the nodal coordinate vector  $\mathbf{n} \in \mathbb{R}^{3n_n}$  for the whole structure:

$$\mathbf{n} = \begin{bmatrix} \mathbf{n}_1^T & \mathbf{n}_2^T & \dots & \mathbf{n}_{n_n}^T \end{bmatrix}^T. \quad (1)$$

The arrangement of bars and strings of the tensegrity structure can be defined as follows. Matrix  $\mathbf{C} \in \mathbb{R}^{n_e \times n_n}$ ,  $n_e$  is the number of bars and strings used to represent the structure topology, whose  $m$ th ( $m = 1, 2, \dots, n_e$ ) entry satisfies:

$$[\mathbf{C}]_{im} = \begin{cases} -1, & m = j \\ 1, & m = k \\ 0, & \text{else} \end{cases}. \quad (2)$$

Thus, the overall structure connectivity matrix  $\mathbf{C} \in \mathbb{R}^{n_e \times n_n}$  can be written as:

$$\mathbf{C} = \begin{bmatrix} \mathbf{C}_1^T & \mathbf{C}_2^T & \dots & \mathbf{C}_{n_e}^T \end{bmatrix}^T. \quad (3)$$

### 2.2. Critical buckling analysis

The tensegrity statics with constraints can be given by a nonlinear finite element method (FEM) based on work from [49] in terms of nodal coordinate vector  $\mathbf{n}$ :

$$\mathbf{E}_a^T \mathbf{K} \mathbf{n} = \mathbf{E}_a^T (\mathbf{f}_{ex} - \mathbf{g}) = \mathbf{w}. \quad (4)$$

where:

$$\mathbf{K} = (\mathbf{C}^T \hat{\mathbf{x}} \mathbf{C}) \otimes \mathbf{I}_3, \quad (5)$$

$$\mathbf{g} = \frac{\mathbf{g}}{2} (|\mathbf{C}|^T \mathbf{m}) \otimes [0 \ 0 \ 1]^T. \quad (6)$$

The tangential stiffness of the tensegrity structure is the first derivative of  $\mathbf{K}\mathbf{n}$  with respect to  $\mathbf{n}$ :

$$\mathbf{K}_T = \frac{\partial(\mathbf{K}\mathbf{n})}{\partial\mathbf{n}} = (\mathbf{C}^T \hat{\mathbf{x}}\mathbf{C}) \otimes \mathbf{I}_3 + \mathbf{A}_1 \hat{\mathbf{E}} \hat{\mathbf{A}} \hat{\mathbf{I}}^{-3} \mathbf{A}_1^T, \quad (7)$$

$$\mathbf{A}_1 = (\mathbf{C}^T \otimes \mathbf{I}_3) b.d. (\mathbf{N}\mathbf{C}^T). \quad (8)$$

The left hand side of Eq. (4) can be written in terms of force density  $\mathbf{x}$  (force per unit length) of the structure members as:

$$\mathbf{E}_a^T \mathbf{K}\mathbf{n} = \mathbf{E}_a^T (\mathbf{C}^T \otimes \mathbf{I}_3) b.d. (\mathbf{N}\mathbf{C}^T) \mathbf{x} = \mathbf{A}_{a1} \mathbf{x} = \mathbf{w}. \quad (9)$$

For a given tensegrity structure, increasing the load increases the chances of the structure buckling globally. The following section presents the force lower bound that causes structure global buckling or critical buckling problem as a generalized eigenvalue problem. Normally, tensegrity structures have self-stress modes; matrix  $\mathbf{A}_{a1}$  is not full column rank. Thus,  $\mathbf{x}$  would have infinite solutions, which is given by [50]:

$$\mathbf{x} = \mathbf{A}_{a1}^+ \mathbf{w} + (\mathbf{I} - \mathbf{A}_{a1}^+ \mathbf{A}_{a1}) \mathbf{z}, \quad (10)$$

where  $\mathbf{A}_{a1}^+$  is the Moore-Penrose inverse of  $\mathbf{A}_{a1}$ ,  $\mathbf{V}_2 = (\mathbf{I} - \mathbf{A}_{a1}^+ \mathbf{A}_{a1})$  is the self-stress modes of tensegrity structures, and  $\mathbf{z}$  is an arbitrary vector. Let the structure taken an initial load  $\mathbf{w}_0$ , the structure will global buckle if we continue increasing the force up to  $\alpha\mathbf{w}_0$ . Defining the external force as  $\mathbf{w} = \alpha\mathbf{w}_0$  with an unknown scalar  $\alpha$  and substituting Eq. (10) into Eq. (7) yields:

$$\mathbf{K}_T = \alpha [\mathbf{C}^T (\widehat{\mathbf{A}_{a1}^+ \mathbf{w}_0}) \mathbf{C}] \otimes \mathbf{I}_3 + [\mathbf{C}^T (\widehat{\mathbf{V}_2 \mathbf{z}}) \mathbf{C}] \otimes \mathbf{I}_3 + \mathbf{A}_{a1} \hat{\mathbf{E}} \hat{\mathbf{A}} \hat{\mathbf{I}}^{-3} \mathbf{A}_{a1}^T \quad (11)$$

$$= \alpha \mathbf{K}_{G1} + \mathbf{K}_{G2} + \mathbf{K}_E, \quad (12)$$

where  $\mathbf{K}_{G1}$  and  $\mathbf{K}_{G2}$  are geometric stiffness matrices generated by external force and pre-stress, and  $\mathbf{K}_E$  is the material stiffness matrix. Therefore, when the structure buckles globally, the ordinary differential equation  $\mathbf{K}_T d\mathbf{n} = 0$  has a non zero solution for which a generalized eigenvalue problem is set to solve for  $\alpha$ :

$$-(\mathbf{K}_{G2} + \mathbf{K}_E) d\mathbf{n} = \alpha \mathbf{K}_{G1} d\mathbf{n}. \quad (13)$$

### 3. Tensegrity Drilling Rig Description

The TAMU tensegrity-based drilling rig structure is primarily composed of the rig derrick, the circulation system, well control systems, a drillstring, the electronic hardware, as shown in Fig.2. The rig was designed based on the loading requirement, motor, and platform size limitations of NASA's 2020 Revolutionary Aerospace Systems Concepts Academic Linkage Special Edition: Moon to Mars Ice & Prospecting Challenge (RASC-AL) [51]. The objective of the 2020 challenge was to design and build hardware that can drill and extract water and assess simulated Martian and Lunar subsurface formations.

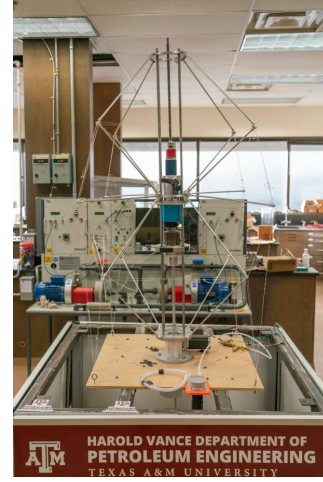


Figure 2: The Tensegrity Drilling Rig.

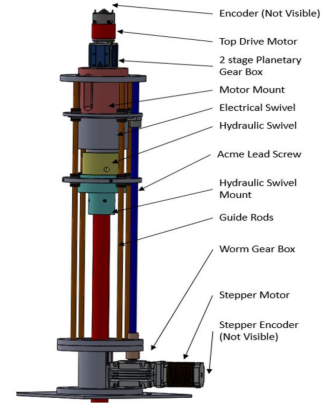


Figure 3: Drilling rig mounting system.

#### 3.1. Rig derrick

The derrick is placed on the base of the drill floor; and is used to carry all loads, raise and lower the drill string, and make connections. The derrick includes the tensegrity structure, ACME rod, rotary motor, gearbox, hydraulic swivel, etc., as shown in Fig.3. A gearbox mount was manufactured to secure the gearbox to the tensegrity rig assembly. The mounting piece was designed to stabilize the motor and drillstring assembly while experiencing excessive vibrations and aiding the system from becoming unbalanced during the drilling operation.

#### 3.2. Tensegrity structure

Most of the drilling equipment in the drilling system is hanging on top of the structure; therefore, requiring mass-efficient structures capable of handling compressive loads while drilling is essential. Tensegrity T-Bar and D-Bar systems have been proven to comply with both requirements, withstanding the compressive loads while being mass-efficient [43]. The three-dimensional T-Bar and D-Bar units as shown in Fig.4, the T-Bar and D-Bar angles (the angles between the sides of the two units and vertical line) are  $\alpha_T = \alpha_D = \frac{\pi}{18}$ . Another advantage of the D-bar

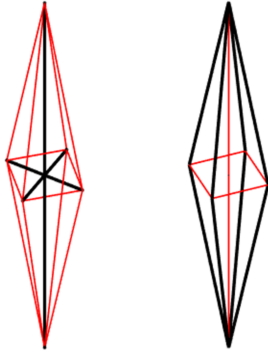


**Figure 4:** Three-dimensional tensegrity T-Bar (left) and D-Bar (right) units with 4 sides, black lines are bars and red lines are strings.

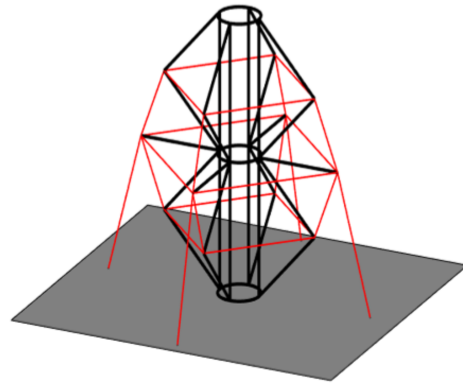


**Figure 6:** Simulation model of the tensegrity rig structure.

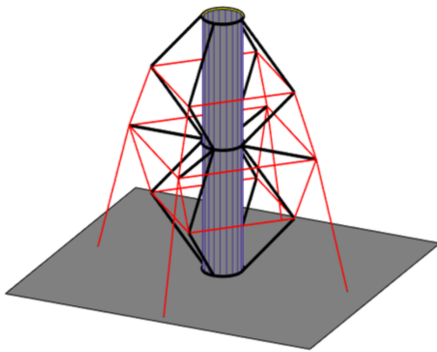


**Figure 5:** Three-dimensional tensegrity  $T_2$  (left) and  $T_2D_1$  (right) structures.

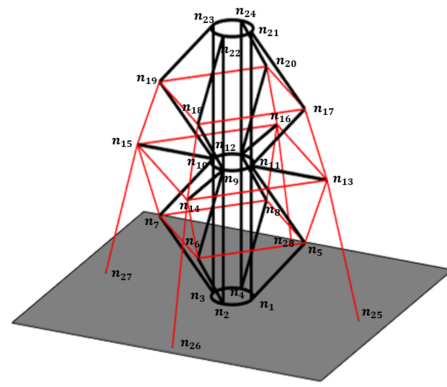


**Figure 7:** Node notation of the tensegrity rig structure, black and red lines are bars and strings.

structure is that one can change its shape by controlling its strings. Thus, at the last iteration of the T-Bar system, we replace the longitudinal bars with D-Bar units such that the overall structure is both deployable and mass efficient [34].

Each longitudinal bar in the T-bar structure can be replaced by another T-bar unit while preserving the structure's total length, which is called a *self-similar rule*. The iteration of the self-similar process times  $q$  is defined as the *complexity* of the structure. Fig.5 on the left shows half of a T-Bar structure of complexity  $q = 2$ . Then, we replace the longitudinal middle bar with two D-Bar units, shown in Fig.5 on the right. To cooperate with the drilling operation structure, we enlarge the middle line with a virtual pipe such that motors move up and down smoothly. The structure configuration is shown in Fig.6, the node notations are shown in Fig.7.

We can break the overall tensegrity into two parts, the table and the tensegrity structure. We chose to build the experimental structure using Hollow Ultra-high Molecular Weight Polyethylene (UHMWPE) aluminum pipes of 0.25in diameter as strings because they provided a lighter weight and higher yield strength than steel. The tensegrity structure is composed of 20 bars and 24 strings in total, as shown in Fig.2. The table is 31in long, 28in wide and 36in tall, making the structure 48in tall, the angles of  $T_2D_1$  structure

**Table 1**

Properties of materials used for the bars and strings.

	Aluminum	Steel	UHMWPE
<b>Yield Stress [Pa]</b>	$1.10e^8$	$3.00e^8$	$2.70e^9$
<b>Young's Modulus [Pa]</b>	$6.00e^{10}$	$2.06e^{11}$	$1.20e^{11}$
<b>Density [kg/m<sup>3</sup>]</b>	$2.7e^3$	$7.87e^3$	$9.7e^3$

are  $\alpha_T = \arctan(\frac{1}{\sqrt{2}})$  and  $\alpha_D = \frac{\pi}{4}$ . More material properties are shown in Table 1.

The developed tensegrity structure (see Fig.2 & 8) is also composed of six unique components: class-1 joint, class-2 joint, ring joint, middle ring, top & bottom rings, and c-section. The bottom & top rings were manufactured to connect the top and bottom halves of the structure to the middle ring. These rings are also effective at housing the railing system. The railing system consists of four guide rails and an ACME rod to allow vertical movement to the drilling rig. All of the tensegrity rings have an inner diameter of 6in to allow the railing system to fit inside the structure and move vertically without interference. The class 1 joint connects the tension strings from the top/bottom c joints and other class 1 joints and anchors them to the tensegrity base. The ring joint is pinned to the top, middle, and bottom rings at the

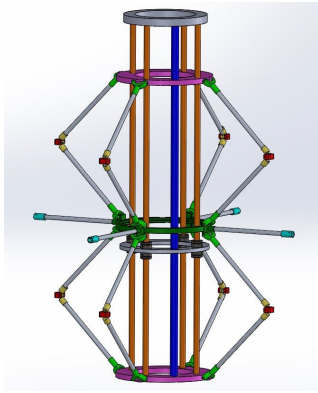


**Figure 8:** Drilling rig with tensegrity network: Tensegrity Skeleton: Ring Joint (green), ACME Rod (blue), Stability Rods (orange), Class 2 Joint (yellow), C-joint (red), Class 1 Joint (aqua).

connecting hubs. The main purpose of the ring joints is to connect a compression bar to the bottom, middle, and top rings. The class-2 joints are utilized as the connection piece for two compression bars. Two class-2 joints are connected by a ball bearing that is situated at the circular cutout. The C section is then pinned to the class 2 joints through the bearings to allow the tension strings to be connected to the other c joints at the same level as the class-1 joint located either above or below. The middle ring consists of four access hubs that allow for two ring joints to be attached. The access hubs for the middle ring also include a female connection for the compression bar that will connect to the class-1 joint. Fig.8 illustrates all of these components being integrated.

### 3.3. Circulation and well control systems

The circulation system includes mud pumps, various mud mixing equipment, mud pits, shale shakers, etc. Drilling fluid is used to circulate rock fragments to the surface, ensure well stability, lubricate, and cool the drill bit. Our design's primary concern was to effectively cool the bit and remove drill cuttings from the system. Thus, other functions were ignored as the system is drilling under atmospheric conditions and a few inches deep into rock blocks. A closed-loop fluid circulation system was utilized with an air valve serving as the source and a shop vacuum serving as the filtration system. A high flow rate vacuum is used to ensure cuttings removal is not a performance limiter, as shown in Fig.3.

Consequently, a blowout preventer (BOP) stack was not required in our rig design; we decided to place a bell nipple between the rig floor and the rock sample. This bell nipple allows sufficient transportation of cuttings from the annular space to the flow line while providing an adequate seal. Another important consideration regarding the drilling fluid circulation system is the design of the swivel placed between the top drive and the drill pipes. The swivel is required to allow simultaneous drilling fluid circulation and drilling string rotation.

### 3.4. Drillstring

The drillstring (shown in Figs.2 & 9) transmits drilling rotation and weight from the surface equipment to the drill bit. It is composed of the drill pipe, a bottom hole assembly (BHA), and the drill bit. The aluminum drill pipe has an outer diameter of 0.375in and a wall thickness of 0.035in. A 1.5in micro bit with 1.48in makeup length was utilized. A cap is connected to the bit and string with a 3/8-18 NPT standard-sized thread on the outside and with a 3/4-32 NPT thread on the inside of the cap that is connected to the BHA sensor capsule. The capsule has 0.9in diameter and functions primarily to mount sensors, protect sensors from circulating fluid, aid sensors in performing accurately and collecting, retrieving, and sending data to the top of the rig for further post-processing. Drillstring faces different forces while drilling. Thus, it is important to assess these properties such as burst strength, fatigue resistance, and compressive-tensile strength to determine the current design's structural limits and avoid pipe failure resulting in damage to the system or operators. Previous tests conducted using the same drillstring have shown that the current drillstring can withstand more than 75 lbs of weight on bit (WOB) without failure and the maximum allowable torque before failure to be about 30 lb-in, beyond which failure of the drill pipe connectors generally occurs [52, 53].



**Figure 9:** Drillstring components, Drillpipe (left), BHA components (right), from [14].

### 3.5. Electronics, hardware, and control

Electronic components are categorized into four sections, 1) sensors, 2) motors, 3) data acquisition, and 4) power requirements.

#### 3.5.1. Sensors

Sensors are used to obtain information about the rock surface for several automation processes, to ensure the system's reliability and efficiency, and to control the safety parameters that the system has to meet. The sensors used in the system were: an Inertial Measurement Unit (IMU); IMUs are devices that measure the exerted force, angular rate, and orientation of a body. In addition, a temperature sensor was included as measuring temperature was crucial to the sensors' data viability as it provided us with information to correct non-linearities on their response (hysteresis).

### 3.5.2. Motors

The rig is equipped with two main motors: the drilling drive (stepper) motor and the top drive (rotary) motor. A-Top Drive Motor is located above the gearbox and controls the rotation and torque of the drill string. The drill string will need higher power input to breach varying terrains. Because of this, the top drive motor is lightweight, and a ball bearing supported, air-cooled, faster, and a more powerful motor. This motor is rated up to 363 Watts and easily connects with the existing gearbox. The motor is installed with spacers to ensure sufficient cooling. b- Drilling Drive Motor: a stepper motor that is used to control the up-down motion (Z motion), which is actuated using a lead-screw (acme) mechanism. Lastly, a precise stepper motor regulated with a two-phase driver and encoder allows for more accurate control of the downward movement of the system and automation of the position of the drillstring.

### 3.5.3. Data acquisition

A data acquisition system is needed to collect, process, and interpret in real-time from the discussed sensors. A slip ring is utilized to convert the rotating wires in the pipe into stationary output wires, thus allowing for wired downhole telemetry. Two Arduino Dues, which run at 84 MHz as a discrete, stand-alone controller for certain rig elements, were utilized, e.g., speed controller's reference followers and high-speed data loggers. The Arduinos were selected because they are cost-effective, replaceable, reliable, and are adequate for real-time control.

### 3.5.4. Power requirement

The drilling rig is powered by a 120VAC power line, while most of the motors and sensors use 12 VDC, which is supplied by a switch-mode power AC/D converter rated for a maximum current draw of 10A.

## 4. Drilling experimental tests

### 4.1. System mounting

A wooden plate was manufactured to attach the tensegrity structure and mount easily to the rig base using steel support pipes with dimensions of 1x1x1 m (see Fig.2). The mounting piece was designed to allow the worm box to be situated under the ACME motor rod. Keeping the cables tense is crucial for the tensegrity structure because it increases its structural strength and stability. Thus, the tensegrity structure was bolted onto the wood support because the tensed cables were situated onto this board, and the eye hooks were fixed to the wooden plate. The wood support was then bolted onto the steel frame to increase the structure's robustness further and to ensure that no slipping occurs from the drilling vibrations.

### 4.2. Drilling operation

The drilling operation started by placing a rock sample at the base of the drilling rig. Then, the topdrive at the top of the structure rotates the drillstring, and the stepper motor and the ACME rod control the up-down motion. This energy (rotation and weight) is transmitted to the drill bit,

which in turn drills rock samples by an indenting and sliding mechanism. Simultaneously, the air is pumped into a swivel and travels through the drill string down to the bit to remove rock fragments and carry cuttings up through the annulus. A t-pipe segment was situated at the borehole to further stabilize and centralize the drillstring and allow for the cuttings to be collected outside the hole in a small tank. The open-loop control algorithms' objective was to drill with faster drilling penetration and low drillstring and structure vibration. The algorithm controls the drilling automation process through the different rock samples by optimizing the rotation and weight provided to the drill bit from the topdrive motor and the stepper motor.

Based on this design and workflow, the tensegrity drilling rig was able to drill several holes of size 1.5-in through different rock formation types such as fluffy sand, consolidated sandstone, and concrete with an average drilling rotation equal to 150-400 revolutions per minute and torque of 3.5-18 ft-lb as shown in Fig.12.

### 4.3. Comparison between tensegrity structure and conventional drilling structure

Based on our drilling tests, tensegrity structure proved to be a minimum mass structure solution for the fundamental loading conditions encountered while drilling. Thus, the tensegrity structure was compared with the conventional lab-scale drilling rig built previously at TAMU (see, Fig.10). The tensegrity structure has a total weight of 8.0 lb. and has a tested hoisting capability equals to 35 lb for lifting multiple motors, rotary union, hydraulic & electric swivels. In addition, the analytical, critical buckling analysis shows that the current hoisting weight (35 lb) is within the safety range of the rig's capability, 292.27 lb, which shows that the developed tensegrity structure can carry loads of approximately 36 times its weight.

It is worth mentioning that the same concept can be applied to a larger scaled size of real rigs. For example, take the Ideal Prime Rig commercialized by National Oilwell Varco, as a reference shown in Fig.11, which has a mast of 142 ft (47.33 m) and a maximum hook load capability of 750,000 lbs. Our validated models show that a proposed tensegrity structure with a mass of 14,300 kg, build using 6.625in OD and 6in ID steel pipes, should be capable of handling the same load (~750k lbs). Consequently, constructing a lightweight full-size tensegrity-based structure for drilling applications on Earth and Mars is not only possible but feasible.

Design variables such as the structure complexity, bar and string sizes, pre-stress in the strings can be tuned using a developed algorithm based on previous work by [34]. For instance, it could be desired to produce a tensegrity rig with different heights, payload, or stiffness constraints subjected to minimal mass design objectives. Nonetheless, the deployment strategy would also require tower cranes for large-scale structures so that the deployable structure can be packaged in rockets for future potential uses on the Moon or Mars.



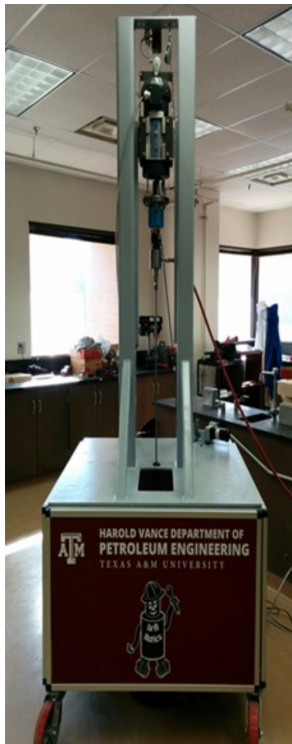


Figure 10: 2019 Drillbotics Rig.

## 5. Conclusions and future work

### 5.1. Conclusions

Based on mathematical modeling and experimental results, we have presented and proved that the tensegrity concept could be applied to unusual applications such as drilling. The conclusions of this paper can be summarized into the following key elements:

1. We proposed a new lightweight drilling structure design using tensegrity concepts for drilling Earth and Martian subsurface formations. Tensegrity design reduces the drilling system weight, improves its mobility, decreases the drilling site's footprint, and allows for more accessible & faster rig installation.
2. A tensegrity-based drilling rig prototype was designed and built to validate our models while drilling through rock under controlled scenarios.
3. A robust model for designing drilling rigs based on tensegrity structures and anticipated load conditions while drilling was presented. Furthermore, our models show that constructing a lightweight tensegrity based structure for drilling applications on Earth and Mars is not only possible but feasible by tuning design variables such as the structure complexity, bar and string sizes, string's pre-stress, etc.
4. Experimental results show that the proposed rig structure is much lighter than a conventional drawworks-based structure and was stable during drilling tests. Moreover, it can carry a load of approximately 36 times its weight. The analytical,



Figure 11: A modern full scale drilling rig used in the oil and gas industry, from [54].

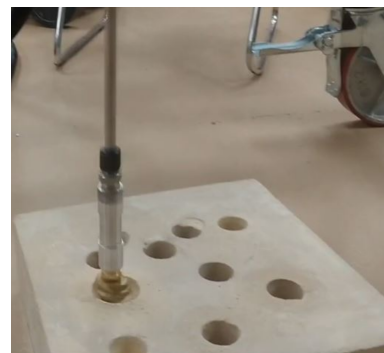
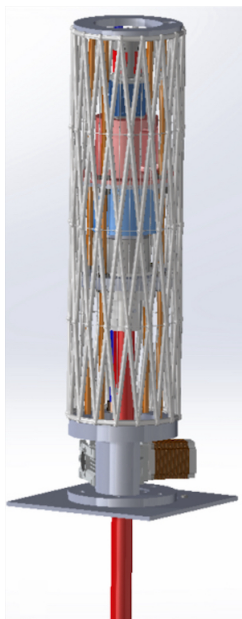


Figure 12: Actual drilling test through sandstone rock.

critical buckling analysis shows the tensegrity rig was hoisting approximately 35 lb, which was by far within the safety range of the rig's hoisting capability of 292.27 lb.

The principles developed in this paper can be used to design and investigate future tensegrity drilling systems for more efficient, safer, and successful drilling operations on Earth and Space. We hope this research brings attention and encourages other researchers to implement tensegrity designs on unconventional systems and novel applications.



**Figure 13:** Initial version of planned Double Helix Tensegrity (DHT) structure.

## 5.2. Future work

- It is planned to use Double Helix Tensegrity (DHT) structure to improve the rig's capability of handling higher torsional loads and forces; this type of structure has been demonstrated to be efficient at handling torques [37]. The DHT structure will also incorporate a new railing system to allow for smoother vertical motion. Fig.13. A shows an initial DHT structure prototype that will be replacing the rig guide rods.
- A Proportional integral derivative (PID) controller will be utilized for the rate of penetration (ROP) optimization based on mechanical specific energy (MSE) concept [55]. A novel rock formation identification technique using machine learning models will also be used while drilling [19]. The purpose of this methodology is to predict rock formation type in real-time while drilling without the need for sophisticated sensors downhole. Drilling data from various sensors are going to be gathered and fed into an Artificial Neural Network and other machine learning classifiers. The algorithms will classify any given formation into one of the six classes - Sand, Clay, Limestone, Concrete, Sandstone, and ice.

## 6. Acknowledgments

Authors acknowledge the financial support from NASA RASC-AL Program, The Energy Institute at Texas A&M, Max Vonderbaum Gift Donation for Drilling Automation Developments, and Gildin's Class of 1975 DVG Developmental Professorship at Texas A&M. Authors acknowledge the support from Texas A&M FEDC and its personnel for timely construction of several parts. Special

mention goes to John Maldonado from the Petroleum Engineering Department at Texas A&M for tremendous help with building activities and last-minute needs.

Authors would like to thank TAMU Automation Team: Srivignesh Srinivasan, Alkassoum Toure, Emily Kincaid, Thomas Lopaz, Jessica Ezemba, Ayodeji Adeniran, Teresa Valdez, Uthej Vattipalli, Le Linh, Ahmed Madi, Narendra Vishnumolakala, Rabih El Helou, and Daniyal Ansari from Texas A&M University for their participation on building the tensegrity rig and sharing their ideas.

We also thank Dr. Sam Noynaert and Dr. George Moridis from Texas A&M University for their valuable suggestions to improve the design. We also appreciate the many helpful discussion on structure buckling analysis with Prof. Shuo Ma, Zhejiang University of Technology.

## References

- [1] A. Fallah, Q. Gu, G. Saini, D. Chen, P. Ashok, E. van Oort, A. Karimi Vajargah, Hole Cleaning Case Studies Analyzed with a Transient Cuttings Transport Model Day 2 Tue, October 27, 2020 (2020). URL: <https://doi.org/10.2118/201461-MS>. doi:10.2118/201461-MS, d021S015R004.
- [2] E. Cayeux, A. Ambrus, L. Øy, A. Helleland, S. Brundtland, H. Nevøy, M. Morys, Analysis of Torsional Stick-Slip Situations from Recorded Downhole Rotational Speed Measurements, SPE Drilling & Completion (2021) 1–15. URL: <https://doi.org/10.2118/199678-PA>. doi:10.2118/199678-PA.
- [3] D. Kaplan, Guest Editorial: Risk Management at NASA and Its Applicability to the Oil and Gas Industry, Journal of Petroleum Technology 68 (2016) 14–15. URL: <https://doi.org/10.2118/1016-0014-JPT>. doi:10.2118/1016-0014-JPT.
- [4] H. Edmundson, Ten Technologies From the 1980s and 1990s That Made Today's Oil and Gas Industry, Journal of Petroleum Technology 71 (2019) 44–48. URL: <https://doi.org/10.2118/0319-0044-JPT>. doi:10.2118/0319-0044-JPT.
- [5] T. Jacobs, The New Pathways of Multiphase Flow Modeling, Journal of Petroleum Technology 67 (2015) 62–68. URL: <https://doi.org/10.2118/0215-0062-JPT>. doi:10.2118/0215-0062-JPT.
- [6] A. A. Deskus, Digitizing E&P: Accelerating the Pace of Change, Journal of Petroleum Technology 66 (2014) 20–23. URL: <https://doi.org/10.2118/0214-0020-JPT>. doi:10.2118/0214-0020-JPT.
- [7] F. E. Dupriest, W. C. Elks, S. Ottesen, P. E. Pastusek, J. R. Zook, C. R. Aphale, Borehole-Quality Design and Practices To Maximize Drill-Rate Performance, SPE Drilling & Completion 26 (2011) 303–316. URL: <https://doi.org/10.2118/134580-PA>. doi:10.2118/134580-PA.
- [8] J. K. Wilson, S. F. Noynaert, Inducing Axial Vibrations in Unconventional Wells: New Insights through Comprehensive Modeling Day 2 Wed, March 15, 2017 (2017). URL: <https://doi.org/10.2118/184635-MS>. doi:10.2118/184635-MS, d022S024R002.
- [9] E. Z. Losoya, et al., Machine Learning Based Intelligent Downhole Drilling Optimization System Using An Electromagnetic Short Hop Bit Dynamic Measurements Day 2 Tue, October 27, 2020 (2020). URL: <https://doi.org/10.2118/201572-MS>. doi:10.2118/201572-MS, d021S011R004.
- [10] T. Jacobs, How Oil Innovation Has Benefited Other Industries, Journal of Petroleum Technology 71 (2019) 40–42. URL: <https://doi.org/10.2118/0319-0040-JPT>. doi:10.2118/0319-0040-JPT.
- [11] R. Beckwith, Drilling in Extreme Environments: Space Drilling and the Oil and Gas Industry, Journal of Petroleum Technology 65 (2013) 56–66. URL: <https://doi.org/10.2118/195803-MS>. doi:10.2118/195803-MS, d021S028R003.
- [12] K. Zaczny, G. Cooper, Considerations, constraints and strategies for drilling on mars, Planetary and Space Science 54 (2006)

- 345–356. URL: <https://www.sciencedirect.com/science/article/pii/S0032063305002515>. doi:<https://doi.org/10.1016/j.pss.2005.12.003>.
- [13] B. Glass, M. New, M. Voytek, Future space drilling and sample acquisition: A collaborative industry-government workshop, *Icarus* 338 (2020) 113378. URL: <https://www.sciencedirect.com/science/article/pii/S0019103519302933>. doi:<https://doi.org/10.1016/j.icarus.2019.07.012>.
- [14] M. Khaled, S. Srinivasan, A. Toure, M. Chen, E. Kincaid, T. Lopaz, L. Rodriguez, J. Ezemba, A. Adeniran, T. Valdez, U. Vattipalli, L. linh, A. Madi, E. Gildin, R. Skelton, S. Noynaert, G. Moridis, Dreams: Drilling and extraction automated system, 2021. arXiv:2106.05874.
- [15] K. Thuot, On the launch pad: the rise of pad drilling, 2014.
- [16] M. K. Bak, Model based design of electro-hydraulic motion control systems for offshore pipe handling equipment (2014).
- [17] C. Carpenter, et al., Real-time analysis for remote operations centers, *Journal of Petroleum Technology* 65 (2013) 160–163.
- [18] A. Wilson, et al., Remote directional drilling and logging in the arctic, *Journal of Petroleum Technology* 69 (2017) 50–51.
- [19] E. Z. Losoya, N. Vishnumolakala, S. F. Noynaert, Z. Medina-Cetina, S. Bukkapatnam, E. Gildin, Automatic Identification of Rock Formation Type While Drilling Using Machine Learning Based Data-Driven Models, IADC/SPE Asia Pacific Drilling Technology Conference and Exhibition Day 1 Tue, June 08, 2021 (2021). URL: <https://doi.org/10.2118/201020-MS>. doi:10.2118/201020-MS.
- [20] C. Bossi, et al., Succeeding in the shale business with a lean well manufacturing management system, *Journal of Petroleum Technology* 69 (2017) 42–44.
- [21] L. F. Wong, B. A. Whiteman, Lightweight drill rod, 1980. US Patent 4,240,652.
- [22] J. Jortveit, Modular light weight drilling rig, 2003. US Patent App. 10/169,929.
- [23] K. Jiang, R. Xie, H. Yun, Lightweight drill pipe based on composite carbon fiber material, in: *Journal of Physics: Conference Series*, volume 1549, IOP Publishing, 2020, p. 032113.
- [24] D. Fan, H. Tian, R. Wang, Development and application of lightweight coring drilling rig in tunnel, *E&ES* 446 (2020) 052005.
- [25] J. Wang, Lightweight electric earth drill, 2020. US Patent 10,689,909.
- [26] R. B. Fuller, Synergetics: explorations in the geometry of thinking, Estate of R. Buckminster Fuller, 1982.
- [27] H. Lalvani, Origins of tensegrity: views of emmerich, fuller and snelson, *International Journal of Space Structures* 11 (1996) 27–27.
- [28] M. Chen, R. E. Skelton, A general approach to minimal mass tensegrity, *Composite Structures* (2020) 112454.
- [29] Z. Kan, N. Song, H. Peng, B. Chen, X. Song, A comprehensive framework for multibody system analysis with clustered cables: examples of tensegrity structures, *International Journal of Solids and Structures* 210 (2021) 289–309.
- [30] T. Bliss, T. Iwasaki, H. Bart-Smith, Central pattern generator control of a tensegrity swimmer, *IEEE/ASME Transactions on Mechatronics* 18 (2012) 586–597.
- [31] A. P. Sabelhaus, H. Zhao, E. L. Zhu, A. K. Agogino, A. M. Agogino, Model-predictive control with inverse statics optimization for tensegrity spine robots, *IEEE Transactions on Control Systems Technology* (2020).
- [32] D. E. Ingber, N. Wang, D. Stamenović, Tensegrity, cellular biophysics, and the mechanics of living systems, *Reports on Progress in Physics* 77 (2014) 046603.
- [33] T. Liedl, B. Högberg, J. Tytell, D. E. Ingber, W. M. Shih, Self-assembly of three-dimensional prestressed tensegrity structures from dna, *Nature nanotechnology* 5 (2010) 520–524.
- [34] M. Chen, R. Goyal, M. Majji, R. E. Skelton, Deployable tensegrity lunar tower, arXiv preprint arXiv:2009.12958 (2020).
- [35] M. Chen, R. Goyal, M. Majji, R. E. Skelton, Design and analysis of a growable artificial gravity space habitat, *Aerospace Science and Technology* 106 (2020) 106–147.
- [36] S. Ma, M. Chen, R. E. Skelton, Design of a new tensegrity cantilever structure, *Composite Structures* (2020) 112188.
- [37] K. Nagase, R. Skelton, Double-helix tensegrity structures, *AIAA Journal* 53 (2015) 847–862.
- [38] G. Carpentieri, R. E. Skelton, F. Fraternali, Minimum mass and optimal complexity of planar tensegrity bridges, *International Journal of Space Structures* 30 (2015) 221–243.
- [39] M. A. Fernández-Ruiz, E. Hernandez-Montes, L. M. Gil-Martin, The octahedron family as a source of tensegrity families: The x-octahedron family, *International Journal of Solids and Structures* 208 (2021) 1–12.
- [40] K. Koohestani, Innovative numerical form-finding of tensegrity structures, *International Journal of Solids and Structures* 206 (2020) 304–313.
- [41] Y. Su, J. Zhang, M. Ohsaki, Y. Wu, Topology optimization and shape design method for large-span tensegrity structures with reciprocal struts, *International Journal of Solids and Structures* 206 (2020) 9–22.
- [42] Y. Wang, X. Xu, Y. Luo, Topology design of general tensegrity with rigid bodies, *International Journal of Solids and Structures* 202 (2020) 278–298.
- [43] R. E. Skelton, M. C. de Oliveira, *Tensegrity systems*, volume 1, Springer, 2009.
- [44] N. Kim Pham, E. A. Peraza Hernandez, Design exploration of a tensegrity-based twisting wing, in: *ASME 2020 International Design Engineering Technical Conferences and Computers and Information in Engineering Conference*, American Society of Mechanical Engineers Digital Collection, 2020.
- [45] Y. Shen, M. Chen, M. Majji, R. E. Skelton, Markov data-based reference tracking of tensegrity morphing airfoils, arXiv preprint arXiv:2010.10710 (2020).
- [46] J. Shintake, D. Zappetti, T. Peter, Y. Ikemoto, D. Floreano, Bio-inspired tensegrity fish robot, in: *2020 IEEE International Conference on Robotics and Automation (ICRA)*, IEEE, 2020, pp. 2887–2892.
- [47] J. W. Booth, O. Cyr-Choinière, J. C. Case, D. Shah, M. C. Yuen, R. Kramer-Bottiglio, Surface actuation and sensing of a tensegrity structure using robotic skins, *Soft Robotics* (2020).
- [48] K. Garanger, I. del Valle, M. Rath, M. Krajewski, U. Raheja, M. Pavone, J. J. Rimoli, Soft tensegrity systems for planetary landing and exploration, arXiv preprint arXiv:2003.10999 (2020).
- [49] S. Ma, M. Chen, R. E. Skelton, Tensegrity system dynamics based on finite element method, 2021. arXiv:2106.02176.
- [50] R. E. Skelton, T. Iwasaki, D. E. Grigoriadis, A unified algebraic approach to control design, CRC Press, 1997.
- [51] T. N. I. of Aerospace (NIA), Revolutionary Aerospace Systems Concepts – Academic Linkage (RASC-AL), 2020. URL: <http://rascal.nianet.org/>.
- [52] C. Geresti, M. Khaled, N. Moosajee, L. Lane, Texas a&m drillbotics 2019 design report, 2019. URL: <https://drillbotics.com/wp-content/uploads/simple-file-list/Design-Reports/Design-Reports-2019/2019-TAMU-Drillbotics-Design-Rpt.pdf>.
- [53] E. Z. Losoya, E. Gildin, S. F. Noynaert, Real-time rate of penetration optimization of an autonomous lab-scale rig using a scheduled-gain pid controller and mechanical specific energy, *IFAC-PapersOnLine* 51 (2018) 56–61. doi:<https://doi.org/10.1016/j.ifacol.2018.06.355>, 3rd IFAC Workshop on Automatic Control in Offshore Oil and Gas Production OOGP 2018.
- [54] NOV, Land Drilling Rigs Portfolio, 2021. URL: <https://www.nov.com/-/media/nov/files/products/rig/rig-equipment/land-drilling-rigs/land-rig-portfolio-catalog.pdf>.
- [55] R. Teale, The concept of specific energy in rock drilling, *International Journal of Rock Mechanics and Mining Sciences & Geomechanics Abstracts* 2 (1965) 5773.